International Journal of Pharmaceutics: X 3 (2021) 100102

Contents lists available at ScienceDirect

International Journal of Pharmaceutics: X

journal homepage: www.sciencedirect.com/journal/international-journal-of-pharmaceutics-x

Compression of amorphous solid dispersions prepared by hot-melt extrusion, spray drying and vacuum drum drying

Barbara V. Schönfeld [a,b], Ulrich Westedt [b], Karl G. Wagner [a,*]

[a] Department of Pharmaceutical Technology, University of Bonn, Gerhard-Domagk-Straße 3, 53121 Bonn, Germany
[b] AbbVie Deutschland GmbH & Co. KG, Knollstraße 50, 67061 Ludwigshafen, Germany

ARTICLE INFO

Keywords:
Ritonavir
Hot-melt extrusion
Spray drying
Vacuum drum drying
Amorphous solid dispersion
Compression analysis
Downstream processing

ABSTRACT

The present study explored vacuum drum drying (VDD) as an alternative technology for amorphous solid dispersions (ASDs) manufacture compared to hot-melt extrusion (HME) and spray drying (SD) focusing on downstream processability (powder properties, compression behavior and tablet performance). Ritonavir (15% w/w) in a copovidone/sorbitan monolaurate matrix was used as ASD model system. The pure ASDs and respective tablet blends (TB) (addition of filler, glidant, lubricant) were investigated. Milled extrudate showed superior powder properties (e.g., flowability, bulk density) compared to VDD and SD, which could be compensated by the addition of 12.9% outer phase. Advantageously, the VDD intermediate was directly compressible, whereas the SD material was not, resulting in tablets with defects based on a high degree of elastic recovery. Compared to HME, the VDD material showed superior tabletability when formulated as TB, resulting in stronger compacts at even lower solid fraction values. Despite the differences in tablet processing, tablets showed similar tablet performance in terms of disintegration and dissolution independent of the ASD origin. In conclusion, VDD is a valid alternative to manufacture ASDs. VDD offered advantageous downstream processability compared to SD: less solvents and process steps required (no second drying), improved powder properties and suitable for direct compression.

1. Introduction

One of the most promising approaches to formulate poorly water soluble drugs is the application of amorphous solid dispersions (ASDs) improving solubility and thus, bioavailability (Démuth et al., 2015). The most common ASD manufacturing technologies used in commercial scale in the pharmaceutical industry are hot-melt extrusion (HME) and spray drying (SD).

However, each manufacturing technique has its own advantages as well as disadvantages and should be chosen based on drug properties (Vasconcelos et al., 2016). Advantages of HME are continuous and solvent-free process, well-known and established technology including availability of modelling and scaling approaches, and cost-efficiency. Disadvantages are limited range of processible polymers and less suitability for APIs with thermal or shear sensitivity (Shah et al., 2013). Additionally, milling of the extrudates is usually required prior to tableting. SD on the other hand is a thermally gentle technology reducing thermal stress related to the evaporation cooling effect (Dobry et al., 2009). Therefore, SD is suitable for thermal and shear sensitive APIs reducing degradation. Disadvantageously, SD is cost-intensive, requiring high amounts of solvents and subsequent drying energy. Furthermore, additional process steps after the drying process are required such as second drying or densification via roller compaction (Haser et al., 2017) to achieve an intermediate suitable for tablet manufacturing.

Several studies investigated the impact of HME and SD on the ASD manufacturability in terms of physico-chemical properties (Patterson et al., 2007), achievable drug load (Dedroog et al., 2019) or suitability

Abbreviations: API, active pharmaceutical ingredient; ASD, amorphous solid dispersion; CP, compaction pressure; D, tablet diameter; f_1, difference factor; f_2, similarity factor; FFC, flow function coefficient; HME, hot-melt extrusion; LOD, loss on drying; na, not applicable; n.d., not determined; P, breaking force; PS_{min}, minimal punch separation; PSD, particle size distribution; RTV, ritonavir; SE, secondary electron; SD, spray drying; SEM, scanning electron microscope; SF, solid fraction; SSA, specific surface area; t, tablet thickness; TER, Total elastic recovery; Tg, glass transition temperature; TS, tensile strength; V, volume; VDD, vacuum drum drying; w, tablet wall height; X-ray μCT, X-ray microcomputed tomography.

* Corresponding author.
E-mail addresses: barbara.schoenfeld@uni-bonn.de (B.V. Schönfeld), ulrich.westedt@abbvie.com (U. Westedt), karl.wagner@uni-bonn.de (K.G. Wagner).

https://doi.org/10.1016/j.ijpx.2021.100102
Received 13 August 2021; Received in revised form 27 October 2021; Accepted 29 October 2021
Available online 3 November 2021

for APIs showing high recrystallization tendency (Haser et al., 2017). Moreover, studies observed differences in resulting ASD powder properties (Huang and Williams, 2018) and downstream processing such as tabletability (Davis et al., 2018; Démuth et al., 2015; Iyer et al., 2013).

Vacuum drum drying (VDD) was recently assessed as a promising alternative technology to prepare ASDs and compared to HME and SD on the ASD intermediate level (Schönfeld et al., 2021). VDD is a well-known drying technology in the food industry (Bhandari et al., 2013), but rarely known in the pharmaceutical field of drug product development. Raghavan and Jett (2004) presented drum drying as new technology for the manufacture of heparin. Whereas Sangekar et al. (2003) introduced drum drying for a molecular dispersion composition with enhanced bioavailability. Based on the functional principle VDD is an interesting technology for manufacturing ASDs especially in comparison to other solvent evaporation-based technologies such as SD. One benefit might be the opportunity to eliminate a second drying step by adjusting the retention time of the material on the heated rotating drums under vacuum. In addition, less solvent consumption conceivably increases cost-efficiency further since even highly viscous liquids can be processed as demonstrated in food industry applications. Consequently, higher solid loads result in higher solid throughputs and thus, lower processing times reducing overall costs. Finally, mild process temperatures combined with vacuum facilitate the processibility of even thermosensitive compounds.

Schönfeld et al. (2021) demonstrated that the solid state of the respective ASDs was similar independent of the ASD manufacturing technology. However, published information on downstream processing including product performance, is missing. Thus, the purpose of this study was to assess if the downstream processing and product performance of an ASD formulation is similar as well. For that, an ASD composition (pure ASD prepared by HME, SD and VDD, and formulated with outer phase excipients) was compared in terms of downstream processing including powder characteristics, compression behavior (tabletability, compactability), tablet morphology (scanning electron microscopy, X-ray microcomputed tomography) and product performance (friability, disintegration, dissolution).

Therefore, ritonavir in a copovidone/sorbitan monolaurate matrix (drug load: 15% w/w) was chosen as model system. Ritonavir exhibits favorable physicochemical properties for a comparative study of different ASD technologies: good solubility in matrix polymer copovidone, and simultaneously, sufficient solubility in common organic solvents while showing low tendency for degradation and low risk for fast recrystallization during processing. Furthermore, a drug load of more than 25% (w/w) limits the ritonavir dissolution as recently demonstrated by Indulkar, 2019. Consequently, ritonavir was selected to ensure manufacturability, since it can be amorphously embedded in a copovidone-based matrix by either HME, SD or VDD resulting in an ASD intermediate with acceptable quality attributes (Schönfeld et al., 2021). And finally, a drug load of 15% (w/w) in the ASD was used to enable detection of any potential impact of ASD manufacturing technology on the quality attribute drug dissolution of the final tablet. To compensate the impact of particle size distribution (PSD) on the corresponding powder properties and compression behavior, the HME material was milled to match the PSD of the VDD intermediate. For comparison, tablet formulations based on ASD intermediates were investigated.

2. Material and methods

2.1. Materials

Ritonavir (purity >99.8%) was obtained from AbbVie Inc. (North Chicago, US). Copovidone (polyvinylpyrrolidone–vinyl acetate copolymer, Kollidon® VA 64) was purchased from BASF SE (Ludwigshafen, Germany), fumed silicon dioxide (Aerosil® 200) from Evonik Industries (Essen, Germany), sorbitan monolaurate (Span® 20) from CRODA (Nettetal, Germany), dicalcium phosphate anhydrous (DI-CAFOS® A60) from Chemische Fabrik Budenheim (Budenheim, Germany), and sodium stearyl fumarate (PRUV®) from JRS Pharma (Rosenberg, Germany). Acetone (Emprove® Essential, purity 96%) and methanol (Emprove® Essential, purity 99.5%) were obtained from Merck KGaA (Darmstadt, Germany).

2.2. Methods

2.2.1. Amorphous solid dispersion (ASD) preparation

Ritonavir (15% w/w) containing amorphous solid dispersions (ASDs) were prepared by hot-melt extrusion (HME), spray drying (SD) and vacuum drum drying (VDD). The composition of the tablets based on ASD intermediates or ASD tablet blends is summarized in Table 1.

2.2.1.1. Hot-melt extrusion (HME). The extrudate beads were kindly provided as benchmark material from AbbVie Deutschland GmbH & Co. KG (Ludwigshafen, Germany). Hot-melt extrusion was performed on a commercial scale co-rotating twin-screw extruder (ZSK 58, Coperion GmbH, Stuttgart, Germany). The extrudate beads were milled using an impact mill (Fitzmill L1A, Fitzpatrick Company, Sint-Niklaas, Belgium) to result in a defined particle size distribution (PSD) comparable to vacuum drum drying intermediate reducing the impact of PSD on e.g., tabletability. To obtain a VDD-like PSD the extrudate beads were initially milled at different conditions, and the resulting milled extrudates were then blended within a glass bottle using a tumble blender (Turbula blender T2C, Willy A. Bachofen AG Maschienenfabrik, Muttenz, Switzerland) for 3 min at 30 rpm. The milled extrudate contained the following extrudate fractions:

- 45% (*w*/w) of extrudate milled at 8000 rpm through 508 µm round-hole sieve,
- 45% (w/w) of extrudate milled at 6800 rpm through 838 µm round-hole sieve,
- 10% (w/w) of sieved extrudate fraction of <63 µm.

2.2.1.2. Spray drying (SD). Ritonavir, copovidone and sorbitan monolaurate were dissolved in a mix of acetone and purified water (90:10 w/w) targeting a solid load of 30% (w/w). Water was added as solvent to reduce electrostatic charging of the final powder, and thus, to ensure tabletability. A Büchi B-290 laboratory spray dryer equipped with an Inert Loop B-295 and a dehumidifier B-296 (Büchi Labortechnik GmbH, Essen, Germany) was used. The spray dryer was operated using a two-fluid nozzle including a 2 mm cap. Following spray drying conditions were applied: feed rate of solution 9 g/min, nitrogen spray gas flow 60 mm (corresponding to 742 l/h), aspirator rate 100% (corresponding to a volume flow of about 35 m^3/h), inlet temperature 65 °C, and resulting outlet temperature 48 °C.

The SD intermediate was subsequently dried for 48 h under vacuum conditions (approx. 50 mbar) at 40 °C using a vacuum oven (Binder GmbH, Tuttlingen, Germany) to ensure complete removal of residual solvents. The residual solvent content for acetone after post-drying was 2339 ppm determined via gas chromatography and thus, below the ICH limit for acetone (EMA/CHMP/ICH/82260/2006, 2019). The throughput (solid) was approximately 100 g per hour.

2.2.1.3. Vacuum drum drying (VDD). Ritonavir, copovidone and sorbitan monolaurate were dissolved in pure methanol (solid load 45% w/w) to obtain the feed solution for VDD. The process was performed in a vacuum double drum dryer (Buflovak, New York, US) equipped with a liquid preparation vessel (TCC-40, TAIM srl, Atessa, Italy) and a peristaltic pump (Watson Marlow 501RL, Watson Marlow, Rommerskirchen, Germany) for liquid feeding (see Fig. 1). The process parameters of the VDD process were set as follows: drum and chasing temperature 80 °C at a pressure of 150 mbar, drum rotation speed 0.2 rpm, drum gap 0.3 mm. The dried product was collected and the

throughput of the solid was approximately 600–700 g per hour. The VDD intermediate was then milled using a screening mill (Comil U5, Quadro Engineering, Waterloo, Canada) equipped with a 991 µm round-hole sieve. The residual solvent content for methanol determined via gas chromatography was below the practical detection limit (< 500 ppm) and thus, below the ICH limit for residual solvents (< 3000 ppm for methanol) immediately after processing not requiring a further drying step.

2.2.2. Tablet blend preparation

The ASD intermediates were supplemented with an outer phase consisting of dicalcium phosphate as filler/binder, fumed silicon dioxide as glidant, and sodium stearyl fumarate as lubricant (see Table 1) according to the Norvir® formulation. The tablet blends were prepared using a tumble blender (Turbula blender T2C, Willy A. Bachofen AG Maschienenfabrik, Muttenz, Switzerland), and a sieve with 1.0 mm mesh size (Retsch GmbH, Haan, Germany) by the following consecutive steps: (1) pre-blending for 3 min at 30 rpm, (2) sieving manually, (3) main blending for 3 min at 30 rpm. The batch size was 100 g each.

2.2.3. Glass transition temperature (Tg) by differential scanning calorimetry (DSC)

Differential Scanning Calorimetry (DSC) measurements were performed using a Mettler-Toledo DSC 1 (Mettler Toledo, Gießen, Germany) equipped with an auto-sampler and a TC100 immersion cooler (Huber Kältemaschinenbau AG, Offenburg, Germany). All DSC samples (ASD intermediates) were scanned at 10 K/min from (−) 20 °C to 150 °C under nitrogen (gas flow 50 ml/min) as open pan method (dry Tg). The results were analyzed with STARe SW (version 16.1) (Mettler Toledo, Gießen, Germany). All samples were measured as duplicates.

2.2.4. Bulk/tapped/particle (pycnometric) density

The tapped density tester (Pharmatest Apparatebau AG, Hamburg, Germany) was used to determine bulk and tapped density according to Ph. Eur. 2.9.34 (method 1). Bulk and tapped density were calculated by the mass and bulk volume occupied by the powder filled into a 250 ml graduated cylinder. The samples were measured as triplicates.

Particle (pycnometric) density was determined using a helium pycnometer (AccuPyc 1340, Micromeritics GmbH, Aachen, Germany) equipped with a 10 cm^3 sample chamber under following conditions: cycle fill pressure set to 134.45 kPa and equilibration rate set to 0.0345 kPa/min. Purging of the sample chamber was conducted 10 times prior to the measurement. For each analysis 5 cycles were performed. All samples were measured as triplicates.

2.2.5. Flowability

ASD intermediates and tablet blends were analyzed regarding their flow properties using a ring shear tester (RST-XS, Dietmar Schulze, Schüttgutmesstechnik, Wolfenbüttel, Germany) equipped with a 31.37 ml cell. Samples were measured at pre-shear normal stresses of 0.250, 0.525, 0.800 and 1 kPa under ambient temperature (approx. 20–22 °C) and humidity (approx. 45–50% RH) in triplicates. Regression analysis was used for data evaluation.

2.2.6. Particle size distribution

The particle size distribution of ASD intermediates were analyzed using a laser diffraction particle size analyzer (Mastersizer 3000, Malvern Instruments GmbH, Herrenberg, Germany). For the measurements, 2–5 g of the samples were used in combination with the dry powder disperser module Aero S. The samples were dispersed with 0 bar pressure. Data were analyzed using the Mastersizer 3000 Software (version 3.71) according to the Fraunhofer approximation. Measurements were performed as triplicates and averaged.

2.2.7. Specific surface area (SSA)

The specific surface area was determined using the Gemini VII (Micromeritics Instrument Corporation, Norcross, United States). The specific surface area was calculated using single point Brunauer-Emmett-Teller (BET) equation from the adsorption data (Brunauer et al., 1938). The samples were analyzed as duplicates.

2.2.8. Loss on drying

Moisture/volatiles content was determined via the loss on drying (LOD) method using a halogen moisture analyzer (HB43-SSD, Mettler-Toledo GmbH, Giessen, Germany). The samples (approximately 5.5.-6.1 g) were heated to 105 °C and held until mass was constant within ±1 mg for 100 s.

2.2.9. Scanning electron microscopy

A scanning electron microscope (SEM) (SU-3500, Hitachi High Technologies, Krefeld, Germany) equipped with a secondary electron detector (SE) was used to visualize the ASD particle morphology, the tablet surface and tablet cross section. The backscattered electron detector (BSE) was used to visualize the distribution of dicalcium phosphate on the TB tablet surface. The powder samples were attached on SEM tubes using carbon conductive tabs (Plano, Wetzlar, Germany), the tablets using conductive silver liquid. All samples except for the samples for BSE analysis were platin-sputtered (at 30 mA for 40 s) under vacuum conditions using a Quorum Q150TS Coater (Quorum Technologies Ltd., Laughton, UK) to enhance electrical conductivity. Images of samples were collected at various magnifications by applying an acceleration voltage of 5 or 10 kV.

2.2.10. Compression analysis

Tablets ($n = 6$) targeting a mass of 200 mg were compressed on a single punch compression simulator (HB-50, Huxley Bertram Engineering Limited, Cambridge, UK) equipped with 10 mm round, flat face tooling for compression analysis. Five compaction pressures were applied ranging from 50 MPa to 250 MPa simulating a production scale tablet press Fette 3090i (61 stations) at different turret speeds to evaluate speed-dependency at 15 rpm and 80 rpm (according to a linear speed of 0.32 m/s and 1.72 m/s, and a dwell time of 19 ms and 3 ms for Euro B tooling). In addition, compression was simulated at a high turret speed (80 rpm) applying pre-compression prior to main compression to investigate the impact on the tensile strength and thus, tabletability. Pre-compression force was kept constant at 4–5 kN.

For compression analysis the compaction pressure (*CP*) was calculated from the applied main compression force and cross-sectional area of the punch (Eq. (1)).

$$CP = \frac{Main\ Compression\ Force\ [N]}{Cross-sectional\ Area\ [mm^2]} \tag{1}$$

The tensile strength (TS) is the mechanical strength of a tablet normalized by its dimensions allowing to compare tablets with different geometries. Depending on the tablet geometry different equations are required to calculate the TS of a tablet.

For round, flat tablets the TS was calculated as described in Eq. (2) (Fell and Newton, 1970):

$$TS = \frac{2P}{\pi D t} \tag{2}$$

in which P is the breaking force, D is the tablet diameter and t is the tablet thickness.

For convex-faced elongated tablets the calculation for the tensile strength is as follows (Eq. (3)) (Pitt and Heasley, 2013):

$$TS = \frac{2}{3}\left(\frac{10\,P}{\pi D^2\left(2.84\frac{t}{D} - 0.126\frac{t}{w} + 3.15\frac{w}{D} + 0.01\right)}\right) \tag{3}$$

in which P is the breaking force, D is the tablet diameter, t is the tablet thickness, and w is the tablet wall height.

Solid fraction (SF) is the apparent density of the tablet (ρ_{app}) divided by particle (pycnometric) density (ρ_{pyc}) of the powder (Eq. (4)):

$$SF = \frac{\rho_{app}}{\rho_{pyc}} = \frac{m}{V\,\rho_{pyc}} \tag{4}$$

The apparent density of the tablet (ρ_{app}) was calculated from the tablet weight divided by the volume of the tablet. Depending on the tablet geometry different equations are required. For round, flat tablets the volume is calculated as described in Eq. (5):

$$V = \pi\, t \left(\frac{D}{2}\right)^2 \tag{5}$$

For convex-faced elongated tablets (18.0 × 9.5 mm) following equation (Eq. (6)) based on vendor's tooling drawing was used to calculate the volume:

$$V = 146.4\ mm^2 \times w \times 260\ mm^3 \tag{6}$$

in which w is the tablet wall height.

The calculated parameters were used to create plots to describe and compare the compression behavior. The tabletability plot (TS vs CP) shows the ability of a powder to be transformed into a tablet with a certain tensile strength under the applied compaction pressure. The compactability plot (TS vs SF) describes the ability of a powder to produce tablets of defined tensile strength under densification (Heckel, 1961).

2.2.11. Elastic recovery

The total elastic recovery (TER) is calculated as follows (Eq. (7)):

$$TER = \frac{t - PS_{min}}{PS_{min}} \times 100 \tag{7}$$

in which t is the tablet thickness out-of-die in mm and PS_{min} is the minimal punch separation in mm.

2.2.12. Tableting

Tablets (n = 30) consisting of either pure ASD intermediates (ASD tablets) or of tablet blends (TB tablets) were manufactured using a single punch compression simulator (HB-50, Huxley Bertram Engineering Limited, Cambridge, UK) equipped with an elongated, biconvex tooling (18.0 × 9.5 mm) (composition see Table 1). The TS of the tablets was kept constant for comparison reasons at 1.2–1.3 MPa.

Tablets were characterized regarding tablet weight (analytical balance, Sartorius BP 61 S-0 CE, Sartorius AG, Goettingen, Germany), thickness and diameter (caliper, Hommel Hercules Werkzeughandel GmbH & Co. KG, Viernheim, Germany) and breaking force (Erweka TBH 125, Erweka GmbH, Heusenstamm, Germany).

2.2.13. X-ray micro computed tomography (X-ray μCT)

The X-ray micro computed tomography scanner (Rigaku CT Lab GX130, Rigaku Americas Holding Company Inc., The Woodlands, USA) equipped with a tungsten source was used to visualize the internal structure of the tablets. Following conditions were applied for analysis: tube voltage 130 kV, tube current 60 μA, resolution 50 μm/pixel (voxel). The collected data were reconstructed using Rigaku software and visualized using Dragonfly software.

2.2.14. Friability

Friability was determined according to Ph. Eur. 2.9.7 using a friability tester (PTF 30 ERA +60 ERA, Pharma Test Apparatebau AG, Hainburg, Germany).

2.2.15. Disintegration

Disintegration test was performed according to Ph. Eur. 2.9.1 (test setup A) using a disintegration tester (ZT 722, Erweka GmbH, Heusenstamm, Germany).

2.2.16. In-vitro dissolution

Dissolution studies were performed using an USP II dissolution tester (paddle method) (Vision Elite 8, Hanson Research, Clatswoeth, US) equipped with an autosampler (AutoPlus Maximizer, Hanson Research, Clatswoeth, US). ASD and TB tablets equivalent to a dosage strength of 100 mg were analyzed (6 replicates). All experiments were performed using 900 ml of 0.06 M polyoxyethylene-10-laurylether in water, at a temperature of 37 °C ± 0.5 °C for 2.5 h in total and at a paddle speed of 75 rpm. Samples (10 ml) were taken at 6 timepoints (15/30/60/90/120/150 min) filtered through a 10 μm cannula filter (ultra-high-molecular-weight polyethylene (UHMWPE)).

For quantification, the samples were analyzed by an ultra-pressure liquid chromatography system (Agilent 1290, Agilent Technologies, Waldbronn, Germany) equipped with a variable wavelength ultraviolet (UV) detector and a reversed phase column (Phenomenex Kinetex C18, 50 × 2.1 mm, 1.7 μm, maintained at 60 °C during measurement). As mobile phases 0.1% trifluoroacetic acid (mobile phase A) and 100% acetonitrile (mobile phase B) were used in a gradient elution procedure (time [min]/mobile phase B in %: 0/5, 1.6/95, 2.2/95, 2.21/5, 2.5/5). For the sample preparation a mix of methanol/acetonitrile/0.1% trifluoroacetic acid (1:1:1 *V*/V%) was used as diluent (dilution factor 2). The injection volume was 5 μl for sampling timepoint 1 and 1 μl for sampling timepoint 2–6. The measurement was performed at 250 nm (bandwidth 4 nm). The retention time of ritonavir was 1.022 min.

To compare dissolution profiles of SD and VDD intermediates with the reference HME, fit factors f_1 and f_2 were calculated (Polli et al., 1997). The difference factor (f_1) calculates the difference between two curves at each time point and displays the relative error (Eq. (8)):

$$f_1 = \left\{ \left[\sum_{t=1}^{n} |R_t - T_t| \right] \Big/ \left[\sum_{t=1}^{n} R_t \right] \right\} \times 100 \tag{8}$$

where n is the number of sampling time points during dissolution testing, R_t is the reference dissolved amount of ritonavir in percentage at timepoint t, and T_t is the dissolved amount of ritonavir in percentage of the test material (SD or VDD) at timepoint t.

The similarity factor f_2 is a measurement of similarity between two curves in percentage (FDA_Guidance, 1997) (Eq.(9)):

$$f_2 = 50 \times log\left\{ \left[1 + \frac{1}{n} \sum_{t=1}^{n} (R_t - T_t)^2 \right]^{-0.5} \times 100 \right\} \tag{9}$$

The difference factor (f_1) should be between 0 and 15 and the similarity factor (f_2) between 50 and 100 for curves to be considered as similar (FDA_Guidance, 1997).

3. Results

3.1. Powder characterization of ASDs and tablet blends (TB)

3.1.1. Particle size distribution (PSD), particle morphology and specific surface area (SSA)

Fig. 2 visualizes the particle size distribution (PSD) and Table 2 shows the d_{10}, d_{50}, d_{90} values of the ASD intermediates. Laser diffraction analysis identified a relatively broad PSD for the VDD intermediate exhibiting a d_{50} of 179 μm. As targeted, the milled extrudate could mimic the VDD PSD adequately resulting in a broad PSD range with a d_{50} of 168 μm. For the SD material a large content of fine particles were detected (d_{50}: 45 μm), approximately three times smaller than the d_{50} of the VDD and HME material.

Scanning electron micrographs (SEM) visualizing the particle morphology of the ASD intermediates confirmed the PSD data determined via laser diffraction (see Fig. 3). The SEM of the milled extrudate showed irregularly shaped particles with a smooth surface in a broad range of particles sizes (Fig. 3, a1–2). SEM images of the SD intermediate showed intact, whole spheres with diameters of approximately less than

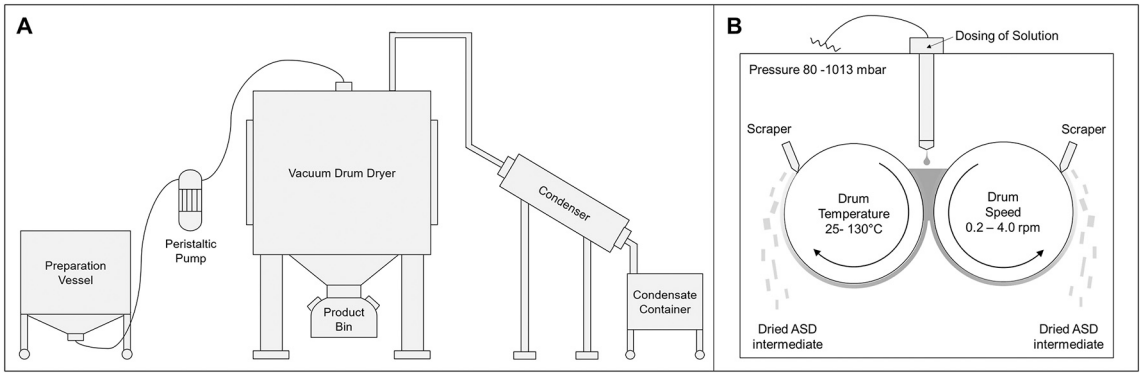

Fig. 1. A: Schematic overview of vacuum drum drying setup. B: Detailed schematic drawing of vacuum drum drying process including parameter ranges.

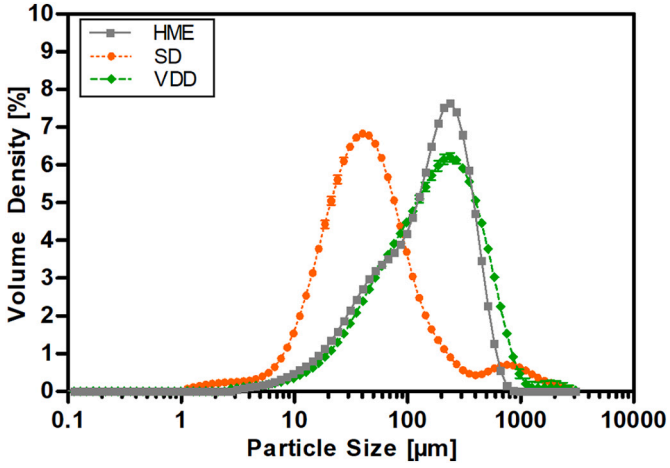

Fig. 2. Particle size distribution of ASD intermediates determined by laser diffraction.

10–50 µm tending to build agglomerates (Fig. 3, b1–2). The VDD intermediate appeared as thin plate-shaped, flaky, irregular particles with sharp breaking edges (Fig. 3, c1–2).

The specific surface area (SSA) results of the ASD intermediates are listed in Table 2. The SSA of the SD intermediate (0.401 m^2/g) was more than three times higher compared to the SSA of the HME (0.119 m^2/g) and slightly higher compared to the VDD intermediate (0.344 m^2/g).

3.1.2. Densities (bulk/tapped/particle (pycnometric)) and flowability

The results of the densities measurements (bulk, tapped, particle) are summarized in Table 2. The particle density values were very similar for all ASD intermediates at around 1.2 g/cm^3, subsequently for the tablet blends at around 1.3 g/cm^3.

The bulk density of the milled extrudate (0.604 g/cm^3) was three times higher than for both solvent-evaporation based materials (SD: 0.226 g/cm^3; VDD: 0.200 g/cm^3). Despite the similar PSD of HME and VDD, higher bulk density was observed for the HME material, which can be explained by the melting of the components during the process resulting in denser and less porous material. Interestingly, the bulk density of SD and VDD was comparable while showing substantially different PSD. This might be explained by the particle form: hollow spherical particles (SD) vs irregular shaped platelets (VDD).

The addition of outer phase excipients (dicalcium phosphate anhydrous, fumed silicon dioxide, sodium stearyl fumarate) to the ASD intermediates resulted in tablet blends with a slightly lower bulk density value for the HME material (HME TB: 0.576 g/cm^3), and slightly higher bulk density values for the solvent-evaporation technologies (SD TB: 0.317 g/cm^3; VDD TB: 0.246 g/cm^3).

Table 2 shows the flowability results assessed based on FFC values determined via ring shear testing. The HME intermediate exhibited easy flowing properties (6.84), whereas the solvent evaporation based ASDs indicated cohesive flow (SD: 2.25; VDD: 3.85). However, the milled VDD intermediate showed a higher FFC value indicating slightly better flowability properties. Notably, a slight increase in FFC at low values between 1 and 4 improves overall processability substantially. The addition of an outer phase to ASDs resulted in tablet blends with FFC values indicating easy flow in all cases (HME: 6.99; SD: 5.64; VDD: 6.92).

3.1.3. Loss on drying (LOD)

The LOD values were within a range of 1–2% (see Table 2). An increase of LOD values after tablet blend preparation was observed for all materials related to the exposure to ambient humidity during

Table 1
Formulation composition of tablets based on ASDs intermediates without outer phase excipients (Tablet (ASD)) and with outer phase excipients (Tablet (Tablet blend)).

Ingredients	Functionality	Tablet (ASD)		Tablet (Tablet Blend)	
		[%w/w]	[mg/tablet]	[%w/w]	[mg/tablet]
Inner Phase (ASD)					
Ritonavir	Active Pharmaceutical Ingredient	15.00	100.0	13.07	100
Copovidone	Carrier Polymer	73.96	493.1	64.42	493.1
Sorbitan monolaurate	Surfactant	10.00	66.7	8.71	66.7
Silicon dioxide*	Glidant	1.04	6.9	0.91	6.9
Outer Phase (OP)					
Dicalcium phosphate anhydrous	Filler	–	–	11.70	89.6
Silicon dioxide	Glidant	–	–	0.90	6.9
Sodium stearyl fumarate	Lubricant	–	–	0.30	2.3
		100.00	666.7	100.00	765.4

* Not used for spray drying and vacuum drum drying; replaced by copovidone.

Table 2
Densities, FFC, particle size distribution, specific surface area, glass transition temperature (dry) and loss on drying values of ASDs manufactured by HME, SD and VDD and their respective tablet blends (n.d.= not determined).

Material	Bulk Density [g/cm^3]	Tapped Density [g/cm^3]	Particle Density [g/cm^3]	Specific Surface Area [m^2/g]	FFC	Particle Size Distribution d_{10} [µm]	d_{50} [µm]	d_{90} [µm]	Loss on Drying [%]	Glass transition temperature (dry) [°C]
ASDs										
HME	0.604 ± 0.009	0.782 ± 0.005	1.201 ± 0.001	0.127 ± 0.011	6.84 ± 0.17 (easy flowing)	32.8 ± 0.41	168.0 ± 1.10	403.0 ± 3.18	1.36	68.2 ± 0.2
SD	0.226 ± 0.009	0.342 ± 0.004	1.196 ± 0.011	0.401 ± 0.010	2.25 ± 0.02 (cohesive flowing)	14.4 ± 0.16	45.3 ± 0.82	188.0 ± 9.38	1.48	67.2 ± 0.2
VDD	0.200 ± 0.001	0.300 ± 0.001	1.194 ± 0.001	0.344 ± 0.000	3.85 ± 0.20 (cohesive flowing)	37.7 ± 0.48	179.0 ± 3.91	530.0 ± 26.6	1.13	68.1 ± 1.3
Tablet Blends										
HME	0.576 ± 0.004	0.794 ± 0.008	1.299 ± 0.001	n.d.	6.99 ± 0.43 (easy flowing)	n.d.			2.01	n.d.
SD	0.317 ± 0.007	0.447 ± 0.003	1.293 ± 0.004	n.d.	5.64 ± 0.26 (easy flowing)	n.d.			1.56	n.d.
VDD	0.246 ± 0.000	0.352 ± 0.001	1.299 ± 0.003	n.d.	6.92 ± 0.71 (easy flowing)	n.d.			1.92	n.d.

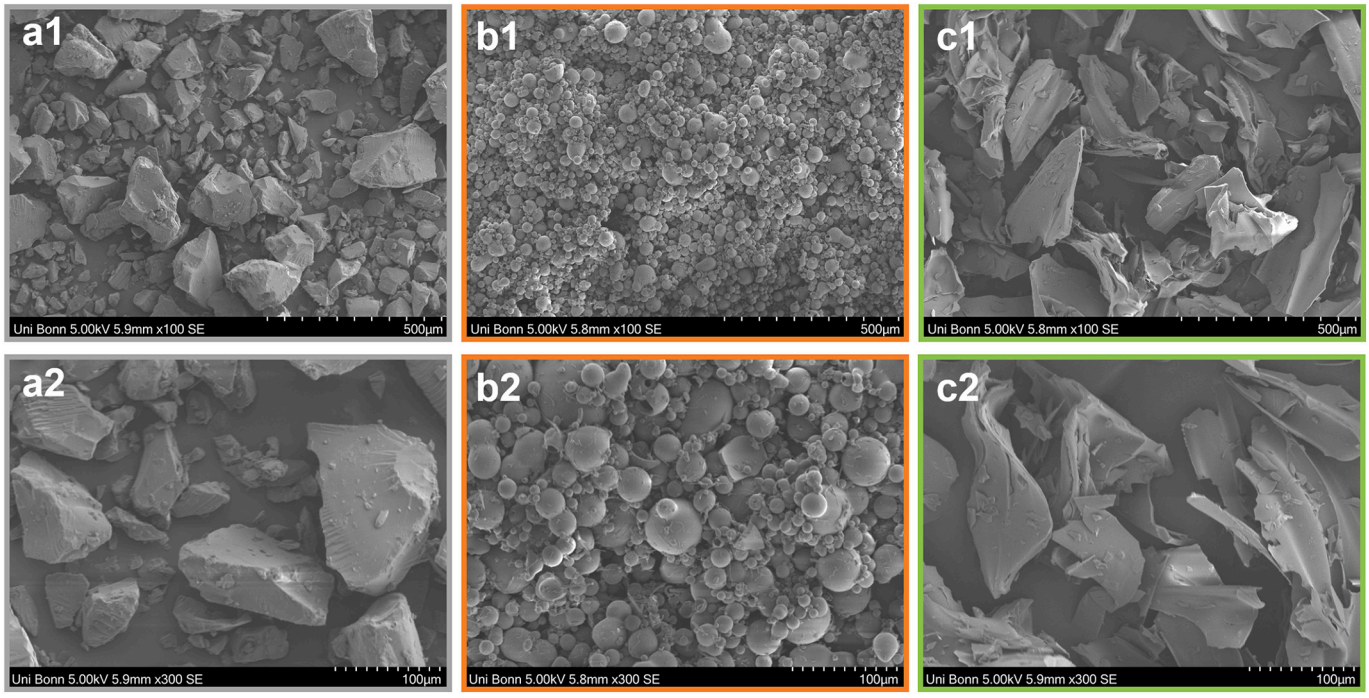

Fig. 3. Scanning electron micrograph images of ASD intermediates at different magnifications: (a) HME; (b) SD; (c) VDD.

processing.

3.1.4. Glass transition temperature (Tg dry)

The glass transition temperatures (Tg dry) of the respective ASD intermediates determined via DSC analysis are summarized in Table 2. All Tg values (dry) were in a comparable range at about 67–69 °C. In addition, all cases showed a single Tg value indicating the API to be molecularly dispersed in the polymer (Lin et al., 2018). Moreover, DSC data indicated the absence of drug substance related residual crystallinity in the ASDs.

3.2. Compression analysis

3.2.1. Tabletability (out-of-die)

Fig. 4 shows the tabletability plots (TS vs CP). The SD material showed unfavorable powder properties such as electrostatic charging (see Section 3.1). Consequently, the die had to be filled manually including unavoidable slightly pre-densification of the powder. Furthermore, simulating the rotary press Fette 3090i at 80 rpm resulted in tablets showing strong capping and/or lamination, which made it impossible to measure tablet dimensions or to determine tablet hardness (see Fig. 4 B). Thus, direct compression of SD intermediate is not feasible in terms of manufacturability.

However, focusing on the ability of the SD powder to be transformed into a tablet not taking the manufacturability into account, the SD

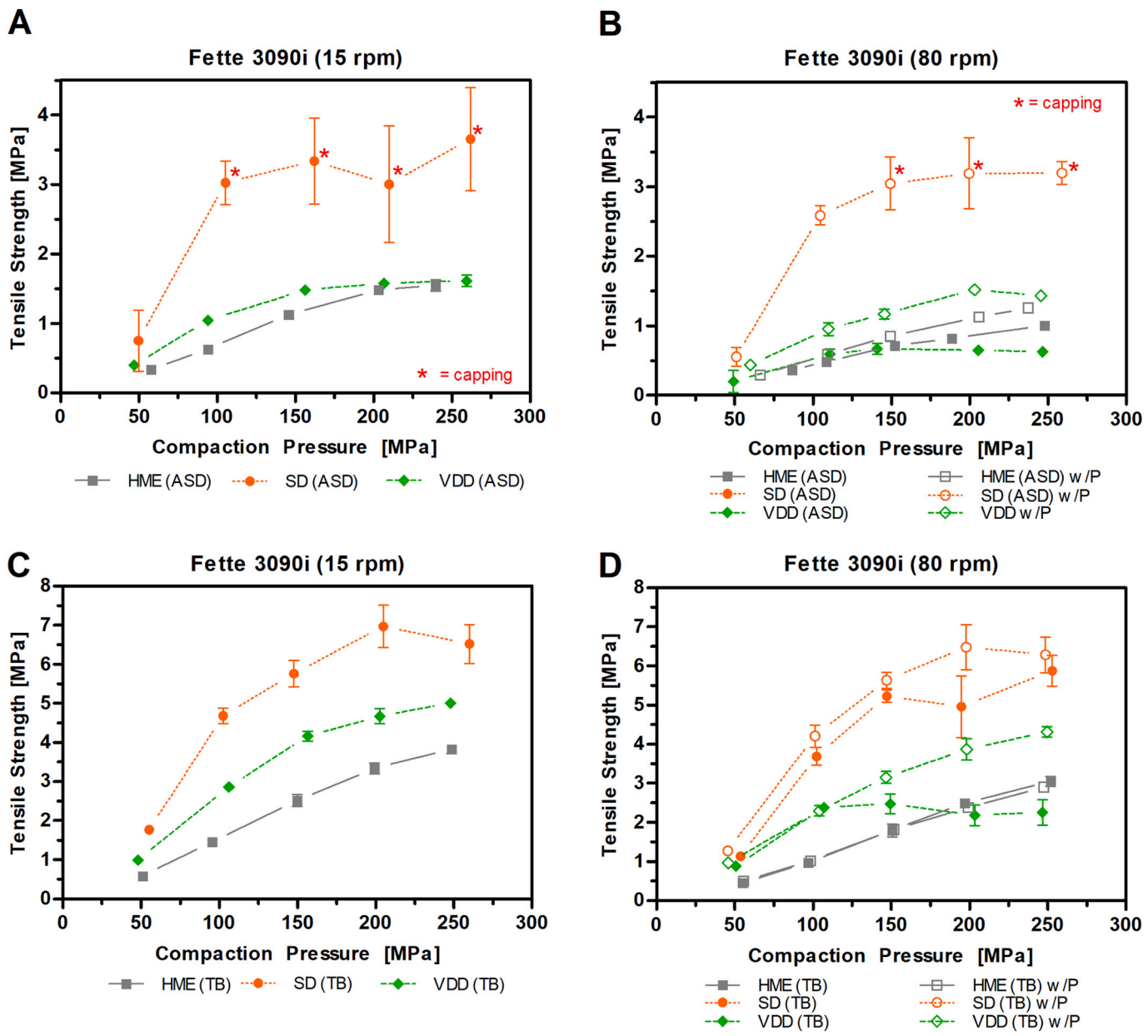

Fig. 4. Tabletability plots: (A, B) ASD tablets; (C, D) TB tablets; (A, C) simulating Fette3090i at 15 rpm; (B, D) simulating Fette3090i at 80 rpm, without and with applied pre-compression force of 4–5 kN (w/P). *Note: SD ASD was manually fed into the die for compression analysis. SD ASD at 80 rpm: not feasible.*

intermediate showed the highest mechanical strength at 15 rpm (TS: 3.6 MPa, see Fig. 4 A) and 80 rpm (TS: 3.2 MPa, see Fig. 4 B) at an applied pre-compression force of 5 kN. Although the weight was kept constant (200 mg ± 10 mg) for compression analysis, the variability of the results for the SD material (both ASD and TB) was high. The maximum TS of the VDD intermediate (TS: 1.6 MPa) was more than twice lower compared to SD. The HME based intermediate resulted in a maximum TS of about 1.5 MPa and thus, similar to the VDD material.

The tabletability plots of the respective tablet blends (see Fig. 4 C + D) showed a shift to higher TSs compared to the pure ASD intermediates. The maximum tensile strength at 15 rpm turret speed for the SD TB was 6.97 MPa, for VDD TB 5.01 MPa, and for HME 3.83 MPa. Moreover, a slight speed dependency could be observed for all ASD intermediates leading to a reduced TS (see Fig. 4 B + D). The strongest impact was observed in case of the SD intermediate leading to strong capping and lamination. Applying pre-compression force affected the solvent-evaporation based ASDs, and respective TBs leading to increased TSs, whereas HME was less affected.

3.2.2. *Compactability (out-of-die)*

Fig. 5 summarizes the compactability plots (TS vs SF) for ASD intermediates (A, B) and tablet blends (TBs) (C, D). The SD intermediate resulted in tablets with low SF values even at high TSs corresponding to high porosity (see Fig. 5 A). In addition, a maximum SF of about 0.89 could be identified even at increasing compaction pressures without increase in TS related to elastic deformation. Tablets based on HME intermediate exhibited the highest SF values (0.95), whereas the VDD intermediate resulted in SF values slightly lower compared to the HME intermediate. Overall, the addition of an outer phase to the ASD intermediates reduced the maximum achievable SF value. However, the data showed that high TS values could be reached at even lower SF values. Consequently, stronger compacts with higher porosity were produced. Higher maximum SF values for the SD TB tablets were noticed compared to the SD ASD tablets.

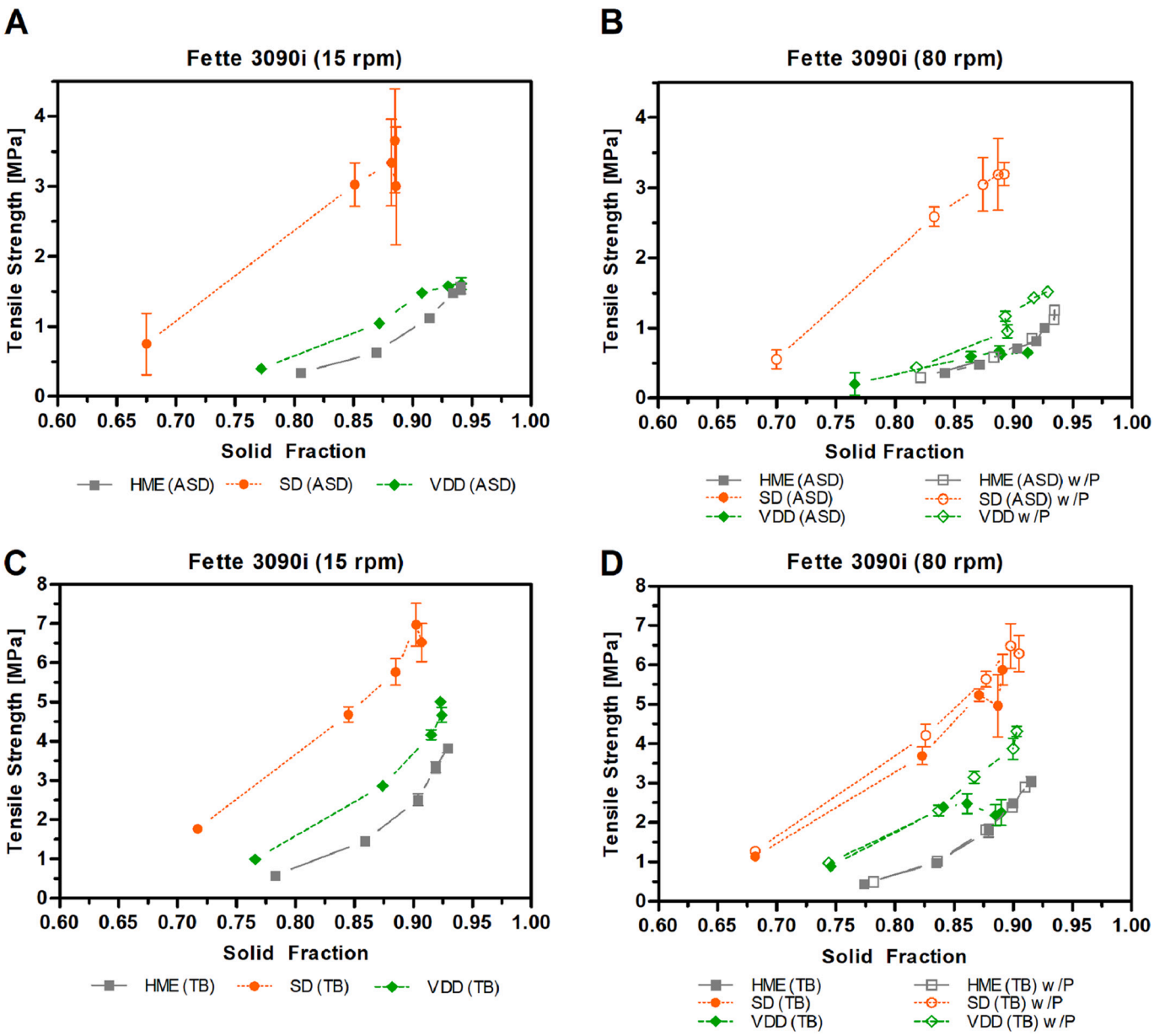

Fig. 5. Compactability plots: (A, B) ASD tablets; (C, D) TB tablets; (A, C) simulating Fette3090i at 15 rpm; (B, D) simulating Fette3090i at 80 rpm without and with applied pre-compression force (w/P). *Note: SD ASD was manually fed into the die for compression analysis. SD ASD at 80 rpm: not feasible.*

Increasing the turret speed caused slight decrease in maximum SF for all ASD intermediates and TBs explicable by the shortened dwell time increasing elastic deformation. However, applying pre-compression force levelled the effect (see Fig. 5 B + D) by increasing dwell time indirectly and by allowing the powder to rearrange within the die.

Compressibility plots are visualized in supplemental data (see Appendix A Fig. S1).

3.2.3. Elastic recovery

Fig. 6 shows the total elastic recovery (TER) of ASD and TB tablets. The TER values raised with increasing compaction pressures in all cases. Comparing ASD based tablets, the SD tablets showed the highest TER values at 15 rpm. The TER values for the HME tablets were lower, whereas the VDD intermediate showed slightly higher TER values compared to the HME intermediate. In addition, with increasing turret speed from 15 to 80 rpm, the TER values increased for all ASD and TB tablets. By adding dicalcium phosphate, all TER values decreased, as well as by applying pre-compression force.

3.3. Tablet characterization

3.3.1. Tablet manufacture

Elongated, biconvex tablets out of ASD and TB were successfully manufactured targeting a dosage strength of 100 mg ritonavir, respectively (Table 4). The aimed common tensile strength of 1.2–1.3 MPa was achieved in all cases. However, the required compaction pressure (CP) values varied depending on the ASD origin: pure HME required the highest CP (283.40 MPa) followed by VDD (127.47 MPa) and SD (69.56 MPa). The total elastic recovery (TER) data were in accordance with the CP values: HME (67.58%) > VDD (30.03%) > SD (15.29%). Regarding tablet porosity, the HME tablets showed the highest SF values (0.97) and the SD ones the lowest (0.80). The VDD tablets were in between with a SF value of 0.93.

The same trends for CF, SF and TER were observed for the TB tablets, although showing substantial lower values generally.

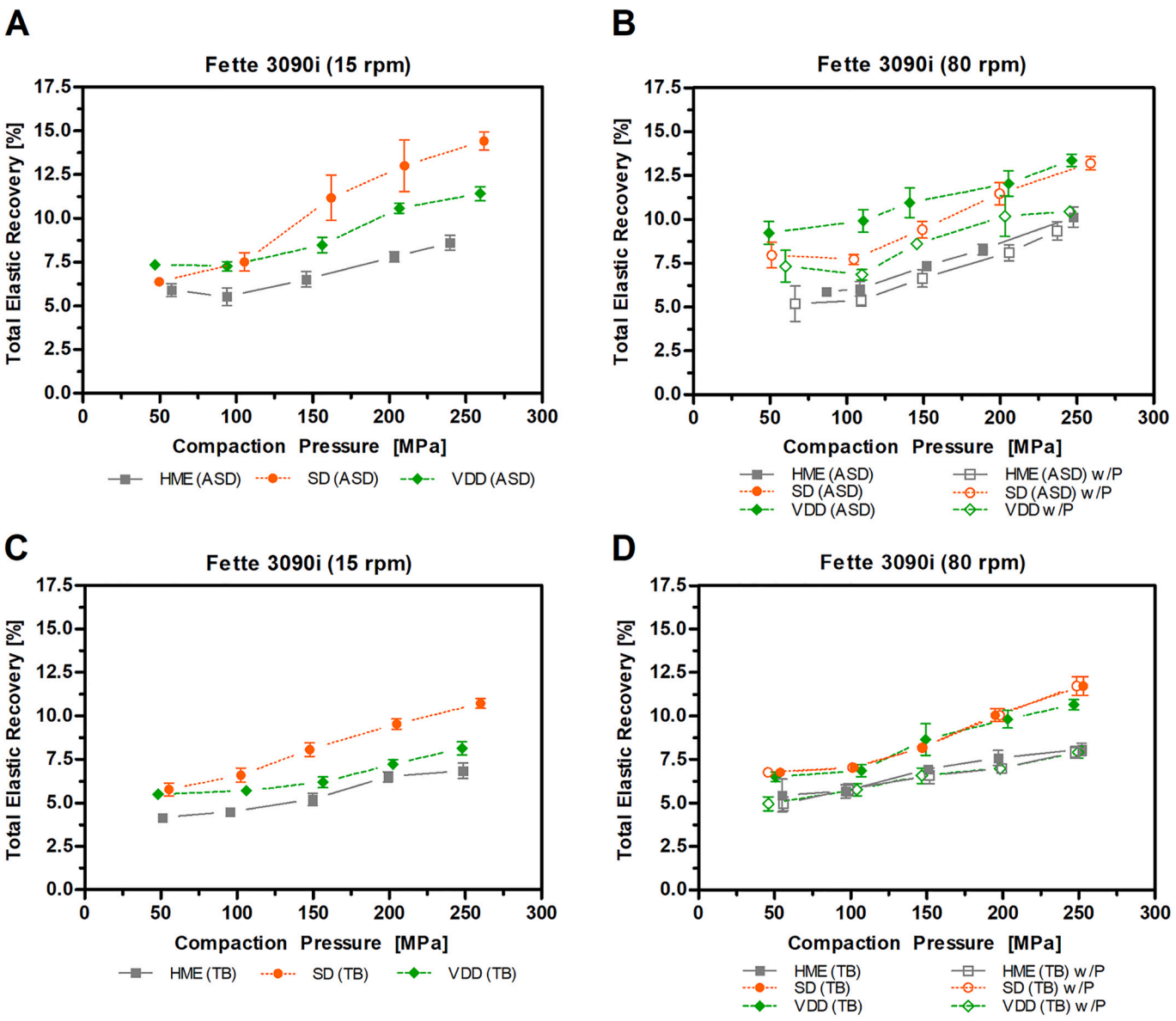

Fig. 6. Total elastic recovery: (A, B) ASD tablets; (C, D) TB tablets; (A, C) simulating Fette3090i at 15 rpm; (B, D) simulating Fette3090i at 80 rpm without and with applied pre-compression force (w/P). *Note: SD ASD was manually fed into the die for compression analysis. SD ASD at 80 rpm: not feasible.*

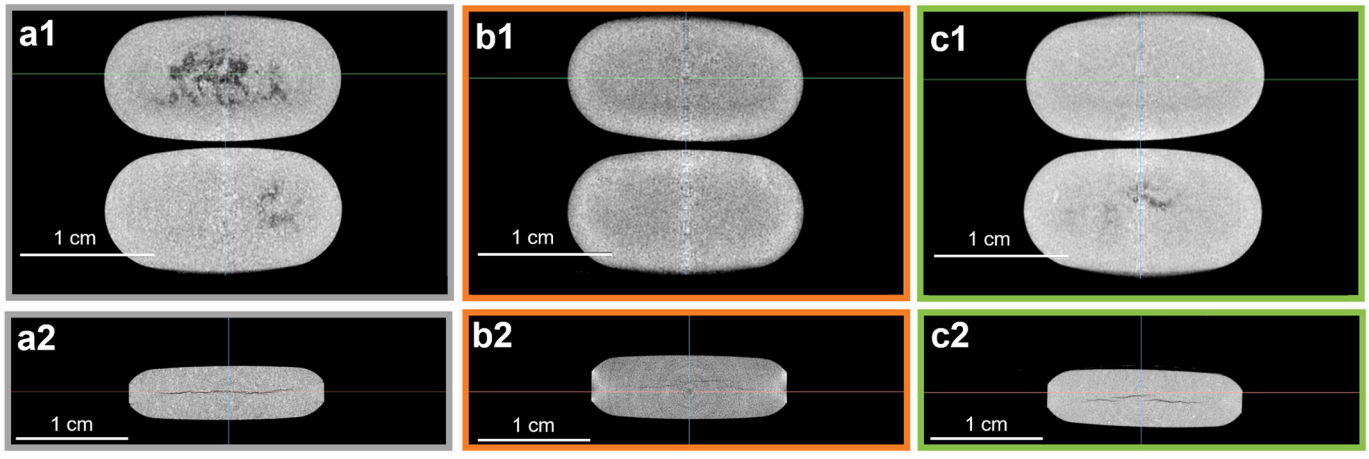

Fig. 7. X-ray µCT images ((1) radial; (2) axial cross section) of ASD tablets: (a) HME; (b) SD; (c) VDD.

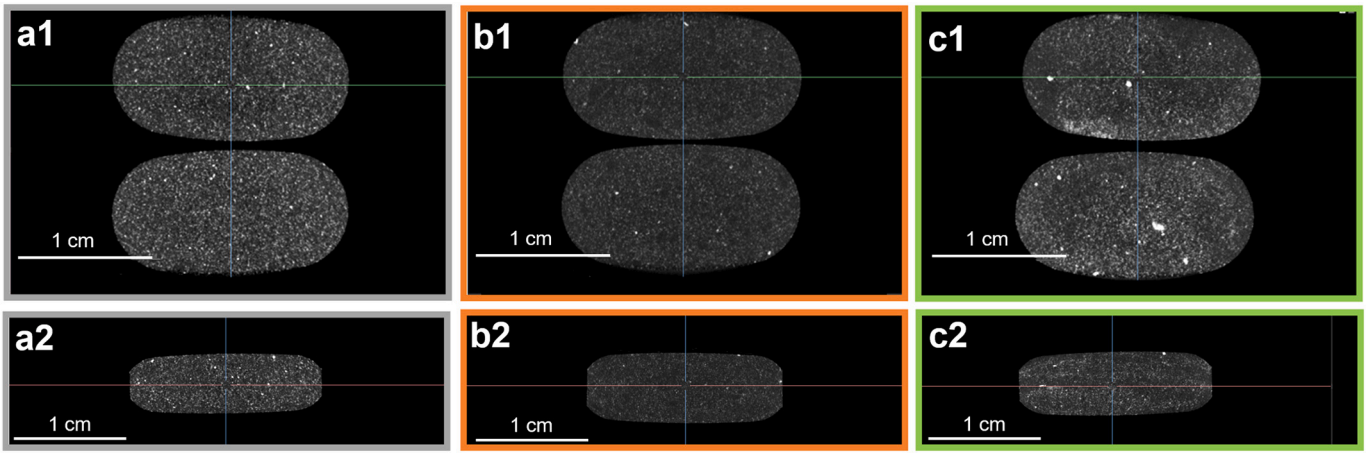

Fig. 8. X-ray μCT images ((1) radial; (2) axial cross section) of TB tablets: (a) HME; (b) SD; (c) VDD.

3.3.2. *Tablet morphology*

The grey scale in the X-ray μCT images is related to the density and the average atomic number of components within the tablet: high density areas are brighter compared to low density areas (e.g. voids) (Neilly et al., 2020). Representative X-ray μCT images show radial and axial cross sections of the tablet midsection for ASD tablets (Fig. 7) and TB tablets (Fig. 8). ASD tablets revealed differences regarding the occurrence of voids: HME tablets (Fig. 7 a1) showed more voids compared to SD (Fig. 7 b1) and VDD tablets (Fig. 7 c1). Moreover, only small voids could be observed within the SD tablet. The axial cross section images revealed cracks within all ASD tablets (Fig. 7 a2, b2, c2). However, tablet defects were not observed for the TB tablets (Fig. 8). Overall, the X-ray μCT images of the TB tablets were darker compared to the ASD tablet images, since the high-dense dicalcium phosphate appeared very bright. Dicalcium phosphate seemed to be homogenously distributed within the HME and SD TB tablets. Whereas the filler within the VDD TB tablet seemed to be less homogenously distributed.

Fig. 9 shows the SEM images of the tablet surface of the ASD tablets. The SD ASD tablet (Fig. 9 b) showed the smoothest surface followed by HME ASD tablet (Fig. 9 a). Slightly higher degree in unevenness could be observed for the VDD ASD tablet related to particle shape (Fig. 9 c). The spherical particles of the SD intermediate were still visible on the smooth tablet surface (Fig. 9 b). However, the SD tablets clearly showed large cracks on the surface across the intact particles. The tablet surfaces of the TB tablets visualizing the dicalcium phosphate distribution are shown in Fig. 10. The filler distribution on the surface of the HME and VDD TBs tablets appeared homogenous. Whereas for the SD TB tablets the surface seemed to be predominantly covered with SD intermediate particles.

Fig. 11 (ASD tablets: a1, b1, c1 and TB tablets: A1, B1, C1) visualizes the SEM images of the respective tablet cross sections. The SEM image of the SD intermediate and SD TB cross section (Fig. 11 b1 and B1) showed mainly intact spheres still present after compression. Interestingly, the wall of the SD spheres seemed to be relatively thick as shown in open, broken spheres. In contrast, the SEM images of the HME intermediate (Fig. 11 a1, A1) revealed compact material without clear edges of

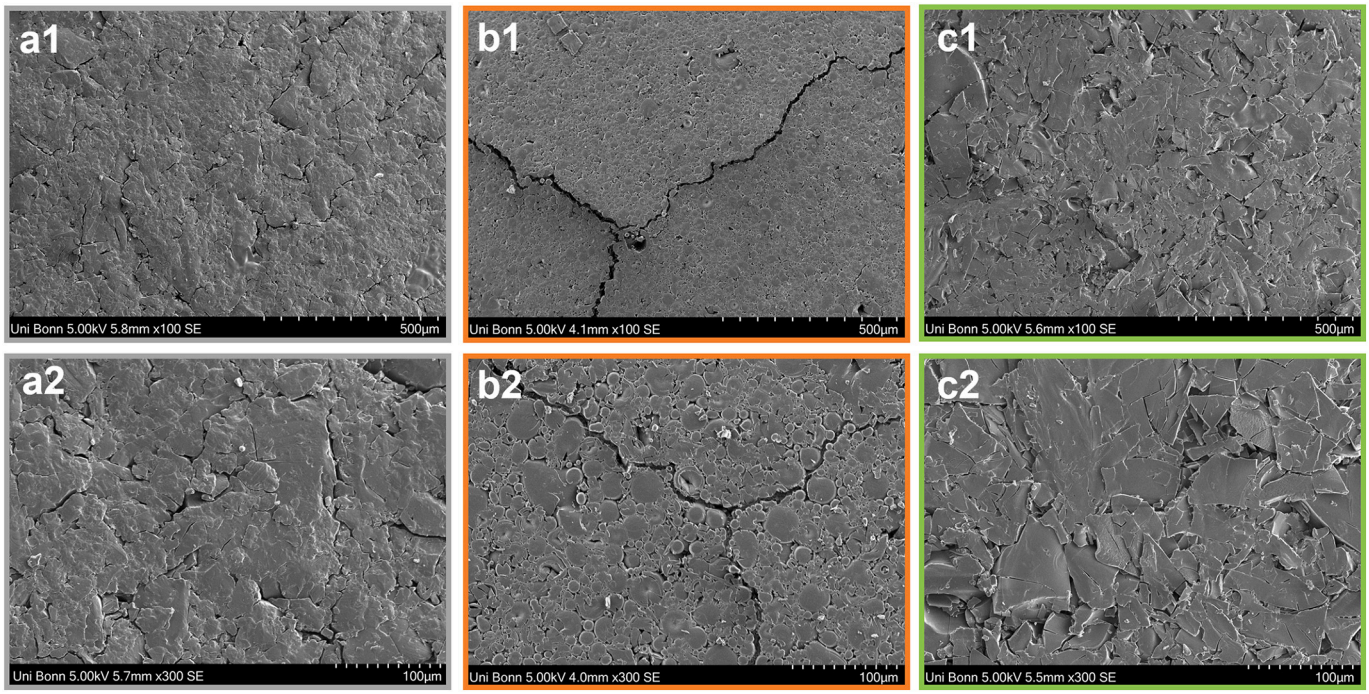

Fig. 9. Scanning electron micrograph images of tablet surface of ASD tablets (at magnification 100× (1), 300× (2)): (a) HME, (b) SD and (c) VDD.

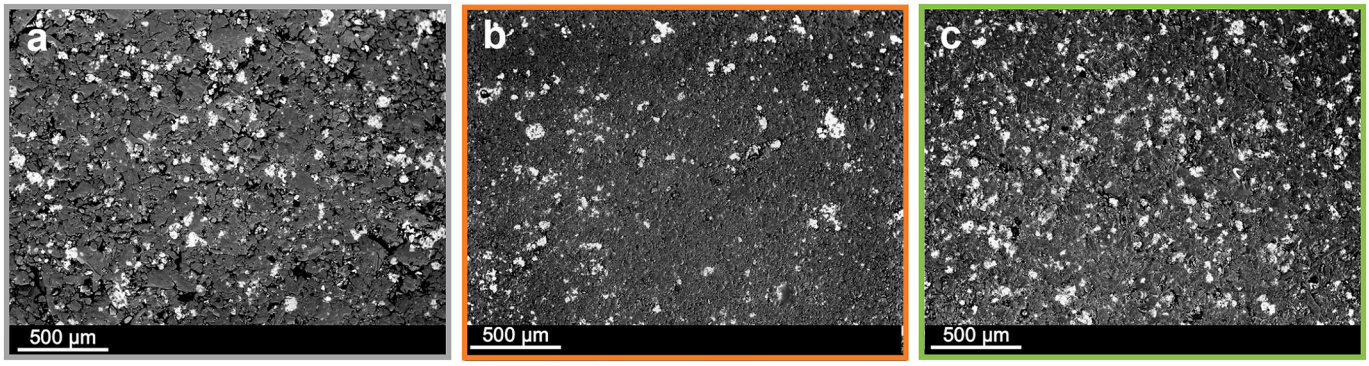

Fig. 10. Scanning electron micrograph images of tablet surface of TB tablets: (a) HME, (c) SD and (d) VDD.

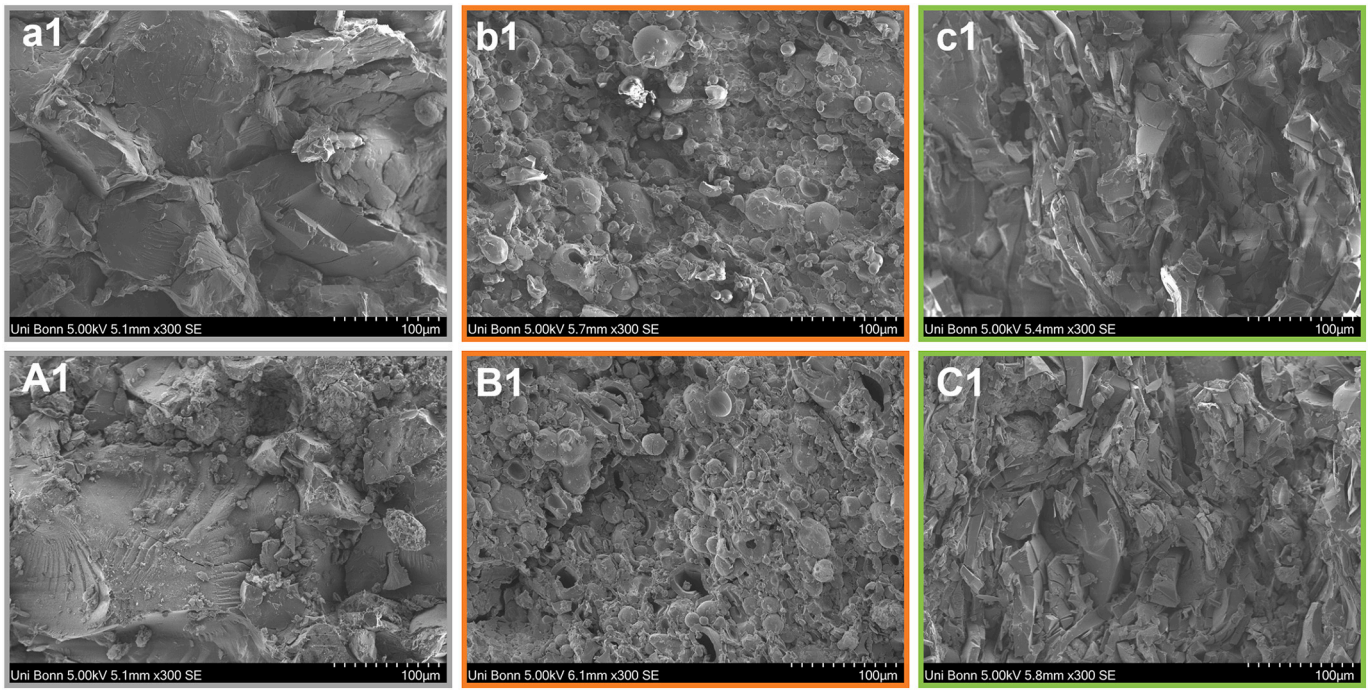

Fig. 11. Scanning electron micrograph images of tablet cross-section of ASD tablets (a1) HME (b) SD and (c) VDD and of TB tablets (A1) HME (B1) SD and (C1) VDD.

Table 3
Results of tablet characterization (elongated, biconvex tooling,18.0 × 9.5 mm) – ASD and TB tablets.

Tablets	Friability [%]	Disintegration Time [min]	Dissolution (ritonavir dissolved) [%]							
			15 min	30min	60 min	90 min	120 min	150 min	F1	F2
ASDs										
HME	0.04	24.2 ± 3.1	49.35 ± 2.75	77.13 ± 2.13	91.26 ± 1.18	91.63 ± 1.21	91.57 ± 1.03	93.76 ± 0.64	Reference	
SD	0.03	29.7 ± 5.2	44.48 ± 2.76	66.44 ± 4.10	90.51 ± 1.71	94.59 ± 1.66	94.28 ± 2.05	95.83 ± 0.99	4.86	65.51
VDD	0.07	28.7 ± 5.0	37.21 ± 4.21	60.60 ± 9.39	88.10 ± 5.82	94.95 ± 1.78	94.81 ± 1.57	95.36 ± 1.85	8.08	54.83
Tablet Blends										
HME	0.11	31.7 ± 5.9	27.99 ± 0.92	47.64 ± 1.54	79.15 ± 1.31	89.58 ± 1.56	91.39 ± 0.93	93.34 ± 0.31	Reference	
SD	0.08	35.8 ± 2.2	40.65 ± 3.93	65.44 ± 4.95	92.83 ± 2.55	95.11 ± 0.78	95.53 ± 1.26	95.27 ± 1.91	13.04	50.34
VDD	0.00	30.2 ± 6.1	36.68 ± 1.09	57.98 ± 0.69	88.38 ± 1.80	90.78 ± 1.99	91.69 ± 1.84	92.66 ± 1.31	7.12	60.10

particles. For the VDD intermediate (Fig. 11 c1, C1) the platelet-shaped particles were still visible. However, the particles led to a coherent compact.

3.3.3. Friability

Table 3 shows the friability results of ASD and TB tablets. The friability results ranged from 0.01% to 0.11% fulfilling the criterion of the European Pharmacopeia (Ph. Eur. (pharmacopoeia) 2.9.7), which states friability below 1% as acceptable.

3.3.4. Disintegration and in-vitro dissolution

Fig. 12 shows the results of the disintegration test. The ASD tablets of similar tensile strength (1.2–1.3 MPa) disintegrated slightly faster (24–30 min) than the TB tablets of similar tensile strength (30–36 min),

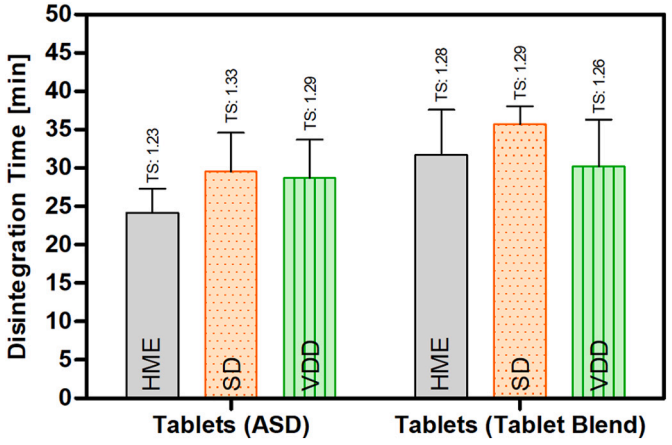

Fig. 12. Disintegration time of tablets consisting of pure ASDs (ASD tablets) and tablets consisting of ASD containing tablet blends (TB tablets) ($n = 6$, TS = tensile strength).

both showing erosion behavior. The statistical significance of the difference between the analyzed tablets was assessed using a one-way analysis of variance (ANOVA) (assumed significance level $\alpha = 0.05$). It can be assumed that the ASD manufacturing technology did not impact the tablet disintegration, because a *p*-value of 0.12 for ASD tablets and 0.19 for TB tablets revealed no significant difference in disintegration time.

Fig. 13 shows the dissolution profiles of ASD tablets (A) and TB tablets (B). In agreement with the disintegration results (see Fig. 12) a slightly slower drug dissolution onset was observed for the TB tablets. However, all tablets showed complete drug dissolution after 120 min. Fit factors (difference factor f_1 and similarity factor f_2) were calculated to assess similarity between dissolution profiles SD and VDD in comparison to HME as reference (see Table 3). ASD tablets showed f_1 values between 0 and 15 (SD: 4.86; VDD: 8.08) and f_2 values between 50 and 100 (SD: 65.51; VDD: 54.83). Consequently, the dissolution profiles could be stated as similar according to the FDA guidance (FDA_Guidance, 1997). The results for the TB tablets revealed similarity for the dissolution profiles as well (f_1 values: 13.04 (SD), 7.12 (VDD); f_2 values: 50.34 (SD), 60.10 (VDD)).

4. Discussion

4.1. Powder characterization ASDs and tablet blends (TB)

The powder characterization of ASDs revealed differences in particle morphology and related powder properties based on the ASD manufacturing technology (Table 2). The milled extrudate is characterized by easy flowing properties, and a high bulk density value leading to an excellent downstream processability (Davis et al., 2018). Both, SD and VDD, showed cohesive flow and an essentially lower bulk density related to the porosity build into the material during solvent evaporation. The SD material tended to agglomerate and showed electrostatic charging both related to the high number of fines resulting in very poor flow despite the favorable spherical particle shape. In addition, the SSA of the SD intermediate was higher compared to HME, which is well-known from literature (Agrawal et al., 2013). Whereas the cohesive flow for the VDD material was expected based on the irregular particle shape (platelets) (Fig. 3 c). Notably, the PSD of the VDD intermediate can be influenced by milling parameters (e.g., screen size, speed) offering the opportunity to design powder properties.

In general, observed differences could be compensated by adding outer phase excipients (filler, glidant, lubricant) and thus, no pronounced difference in terms of flowability could be observed enabling further downstream processing of tablet formulations.

The increased bulk density of the SD and VDD TBs can be explained by the addition of approx. 11.7% (w/w) dicalcium phosphate exhibiting a high bulk density itself. Furthermore, the addition of fumed silicon dioxide as glidant reduced the interparticular friction and decreased surface charge both beneficial for better flow and thus, higher bulk density (Gold et al., 1966; Tran et al., 2019; Varthalis and Pilpel, 1977). The already favorable particle shape, size, and density of the milled extrudate was not improved by the addition of an outer phase.

4.2. Compression analysis

The compression analysis revealed differences in compression behavior of the ASD intermediates with respect to the manufacturing technology used (see Fig. 4, Fig. 5 and Fig. 6). The particle morphology (SSA, PSD, porosity, particle shape) seemed to be crucial independently from the ASD manufacturing technology category (fusion based vs solvent based). Moreover, no Tg related differences could be observed as Tg was similar for all ASDs (67–69 °C, Table 2).

The higher the SSA, the higher the bonding area increasing the mechanical strength of the compacts. Consequently, the SD intermediate showing higher SSA values and high amount of fine spherical particles produced stronger compacts compared to VDD and HME at similar

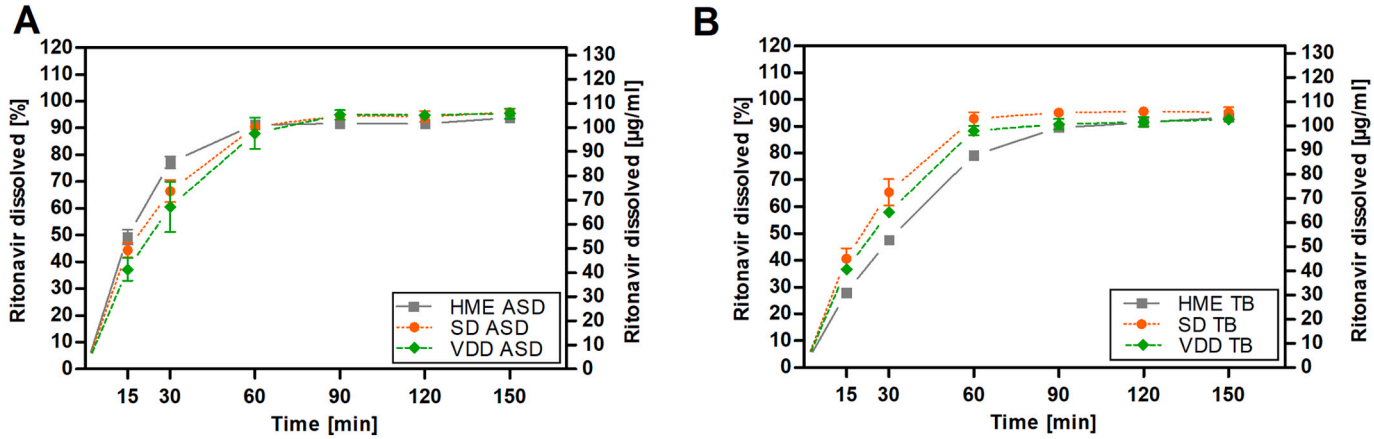

Fig. 13. Dissolution profiles of (A) ASD tablets and (B) TB tablets using USP II paddle method at 75 rpm and non-sink conditions in 900 ml 0.06 M polyoxyethylene-10-laurylether (37 °C ± 0.5 °C) (n = 6).

compaction pressures in the present study, which was also reported for itraconazole containing ASDs in literature (Davis et al., 2018, Olsson and Nyström, 2001). Comparing HME and VDD, the SSA for VDD was higher despite the widely comparable PSDs. Hence, the VDD material showed a higher degree of inner porosity, which was underlined by the bulk density results and could be explained by the manufacturing process itself. Melting the components during hot-melt extrusion combined with applying vacuum ended up in a compact and dense material without air entrapment, whereas the VDD material got perforated during the VDD process due to solvent evaporation resulting in higher SSA and higher degree of inner porosity. Thus, the VDD material showed better tabletability resulting in stronger compacts compared to HME.

The thin irregular-shaped platelets of the VDD intermediate might behave anisotropically during compression in contrast to the rather isotropic, spherical HME particles. This assumption could be underlined by the TER values, which were higher for the VDD material in contrast to HME. In addition, the VDD material might fragment more easily compared to the compact, high-dense HME gravel-like particles due to the high inner porosity of the VDD material, increasing the bonding area under compression leading to higher TS values. In contrast to HME and VDD material, the SD particles were hollow, spherical particles exhibiting thick walls as shown in the SEM images (Fig. 2 and Fig. 11). These gas-filled hollow spheres were exhibiting a high fraction of elastic deformation, which was spontaneously released after ejection of the tablet resulting in tablet defects such as capping. The high degree in elastic recovery was confirmed by TER values (when compared at identical compaction pressure).

Moreover, slight speed dependency in tabletability could be observed for all ASDs independent of the ASD origin, which is likely related to viscoelastic deformation based on high amount of polymer in the formulation (74% w/w).

Applying pre-compression prior to main compression increased TSs of the VDD tablets while enabling tablet processing for the SD intermediate. The impact on HME tablets was less pronounced. In addition, pre-compression force seemed to expand the design space of the compression speed applicable for solvent based ASD intermediates increasing the throughput.

Overall, the addition of an outer phase improved tablet processing by enhancing flowability and tabletability. Exemplarily, the SD TB could be filled automatically resulting in tablets without defects. Moreover, stronger compacts were achieved in all cases at comparable compaction pressure values showing less total elastic recovery.

4.3. Tablet characterization

Elongated, biconvex tablets (18.0 × 9.5 mm) with a dosage strength of 100 mg showed differences in required compaction pressures to reach at target TS of 1.2–1.3 MPa, as well as differences in resulting SF and TER values (Table 4). The trend in required compaction pressures was in accordance with the compression analysis data (e.g., tabletability plots see Fig. 4). However, higher CP values and higher TER values for the ASD tablets were observed indicating over-compression, which is known to result in high elastic recovery and thus, in tablet defects as confirmed via μCT (Fig. 7) and SEM images (Fig. 9). These observations differing from the compression analysis data might be related to the tooling (elongated tooling vs round biplane). As expected, voids could be found in the middle part of the tablets, since the relative density of the tablet is known to be lower in the tablet center for biconvex tablets (Diarra et al., 2015; Eiliazadeh et al., 2003). This effect can be explained by die wall friction enhanced in absence of lubricant in the ASD tablet. Therefore, laminar movement of particles was hindered by wall friction resulting in density distribution differences. Eiliazadeh et al. (2003) observed increasing elastic recovery with increasing density distribution differences between edge and center of the tablet. The present study confirmed this observation. In addition, the μCT images (axial cross section, Fig. 10) revealed cracks within all ASD tablets. These cracks might be related to elastic recovery based on density differences as described above and/or to air entrapment phenomena.Mazel et. (2015) stated that air entrapment could lead to lamination and cracks and that the lamination tendency increases with increasing tablet thickness, compression speed and compaction pressure.

Moreover, for the ASD tablets, the interparticle bonding might not accommodate the elastic recovery at such high compaction pressures to achieve a common tensile strength of 1.2–1.3 MPa resulting in over-compression. Once the compaction pressure is removed, the elastic relaxation induced the bonds to break, diminishing the tensile strength. To reduce the probability of micro-cracking related to elastic recovery, a tapered die could be used allowing the tablet to expand radially (Garner et., 2014). Furthermore, applying pre-compression force or changing the tooling geometry to a tooling with less curvature could be beneficial to avoid lamination as well as increasing the dwell time by reducing tableting speed or changing the punch head configuration (Euro-B to Euro-D).

However, cracks/lamination as well as large voids were not observed for the TB tablets (Fig. 8 and Fig. 10). Obviously, the addition of the filler dicalcium phosphate anhydrous increased the interparticle bonding leading to lower required compaction pressures and thus, less elastic recovery. Moreover, the selection of a brittle filler was beneficial to reduce elastic recovery since brittle fillers themselves show no to minimum elastic recovery. The addition of lubricant also reduced the die wall friction allowing particle movement during compression, which is beneficial especially for convex faced tooling. At the same time, the brittle material dicalcium phosphate anhydrous would balance potential lubricant sensitivity of the non-brittle and potentially lubricant sensitive ASD material.

Interestingly, SD ASD tablets exhibited the lowest SF values (Table 4) and thus, the highest porosity, despite without visible larger voids in the μCT images (Fig. 7b). This observation can be explained by the SEM images of the tablet cross-sections: the hollow spherical SD particles remained mostly intact after compression exhibiting elastic deformation similar to a tennis ball. This phenomenon can be explained by the relatively thick walls of the SD hollows (Fig. 11b) in combination with entrapped air within the spherical particles. This consequently resulted in tablets of reduced density compared to HME tablets.

The distribution of the filler on the surface of the HME and VDD TBs tablets appeared homogenous (Fig. 10). Whereas for the SD TB tablets

Table 4
Results of the tablet manufacture (elongated, biconvex tooling,18.0 × 9.5 mm) – ASD and TB tablets.

Tablets	Weight [mg]	Compaction Pressure [MPa]	Tensile Strength [MPa]	Solid fraction	Total Elastic Recovery [%]
ASDs					
HME	671.2 ± 4.5	283.40 ± 9.43	1.23 ± 0.00	0.97 ± 0.00	67.58 ± 2.24
SD	664.9 ± 4.1	69.56 ± 1.44	1.33 ± 0.06	0.80 ± 0.00	15.29 ± 0.59
VDD	661.4 ± 7.9	127.47 ± 8.77	1.29 ± 0.02	0.93 ± 0.01	30.03 ± 1.41
Tablet Blends					
HME	763.3 ± 4.0	93.94 ± 2.61	1.28 ± 0.09	0.89 ± 0.00	18.78 ± 0.56
SD	761.2 ± 4.3	57.54 ± 0.97	1.29 ± 0.09	0.75 ± 0.00	12.89 ± 0.38
VDD	768.1 ± 3.0	67.64 ± 2.89	1.26 ± 0.02	0.84 ± 0.00	14.67 ± 0.72

the surface seemed to be predominantly covered with SD intermediate particles probably due to the electrostatic charging of the fine SD particles of low density (Fig. 2). However, the Xray μCT images (Fig. 8) of the cross-section within the middle of the tablet revealed a homogenous distribution of the filler within the SD tablet.

Despite the differences in powder and tablet morphology the present study indicates no pronounced differences in tablet performance with respect to friability, disintegration, and dissolution (Table 3) when compressed to similar TSs (1.2–1.3 MPa). In agreement with the disintegration data, the dissolution profiles showed slightly slower drug dissolution onset for the TB tablets, which might be related to the addition of the water-insoluble dicalcium phosphate as filler, and to the absence of voids/cracks within TB tablets hindering water to penetrate the tablets. In accordance with the present study, Indulkar et al. (2019) demonstrated complete drug release for ritonavir/copovidone containing ASD tablets at a drug load below 25% within 30 min. In addition, an initial lag time was observed comparable to the present dissolution profiles. Moreover, the SD and VDD TB tablets showed a slightly faster onset compared to the HME TB tablets, which might be related to the lower relative density (low SF values) of the tablets and thus, higher porosity (Table 4). The tablets were slightly floating above the vessel bottom compared to the HME based tablets. Consequently, the SD and VDD tablets surfaces were all over in contact with the dissolution medium. However, at the end of dissolution testing no difference could be observed.

5. Conclusion

The present study revealed differences in powder properties as well as in compression behavior of ASD intermediates in dependence of the manufacturing technology (HME, SD, VDD) despite the similar solid state. Thus, the solid state of an ASD might not be exclusively determining for the downstream processibility and compression behavior in the respective case. Indeed, those differences in material properties could be linked to particle morphology, as the solid state was quite similar in terms of Tg. The HME ASD consisting of large particles of high particle density showed superior powder flow and bulk density while exhibiting less favorable compression behavior such as lower overall tabletability and the need of high compaction pressures to reach sufficient TS values. In contrast, the SD material consisting of fine, hollow-spherical particles showed cohesive flow and electrostatic charging while exhibiting the best tabletability at worst manufacturability (high degree in tablet defects, e.g., capping). Interestingly, the VDD intermediate showed acceptable flow at comparable low bulk density, while exhibiting good tabletability and manufacturability. By adding the brittle filler dicalcium phosphate anhydrous in the outer phase to the ASD intermediates, the described differences were diminished.

Tablet performance such as disintegration and dissolution indicated no quality related differences between tablets consisting of either ASDs alone or tablet blends. Thus, the decision on the appropriate technology for a respective compound could be made individually based on the physico-chemical properties of the compound (e.g., chemical stability, melting point, solubility in solvents) or based on business-related aspects such as inhouse scale-up options. In the current case, HME can be stated as technology of choice for the respective formulation considering economic (e.g., high throughputs) and environmental aspects (e.g., no solvents used) next to material properties and compression behavior. Thus, it is no surprise that the ASD formulation studied here is commercially manufactured via hot-melt extrusion (Norvir® Tablet). However, comparing both solvent-evaporation based technologies the VDD showed benefits, which should be considered: residual solvents amount within limits even without second drying step, higher solid loads feasible to be processed due to less viscosity limitations (45% w/w compared to 30% w/w) as shown in the applications of the food industry and thus, lower solvent consumption. In addition, an ASD via VDD showed direct tabletability for the present formulation offering a broader process window for tableting speed resulting in higher throughputs. Thus, presumably eliminating process steps while requiring lower overall footprint in production scale makes the VDD cost-effective and attractive for the pharmaceutical industry.

Indeed, further experiments using the new technology vacuum drum drying should be considered in future to increase process understanding by assessing the interplay between process parameters and critical quality attributes in more detail.

Acknowledgments & funding

The authors kindly thank Thilo Faber (University of Bonn) for his technical assistance in scanning electron microscopy, John Roth (AbbVie Inc. North Chicago USA) for X-ray μCT analysis support and Andrew Vogt (AbbVie Inc. North Chicago USA) for specific surface area analysis support.

This work was funded by AbbVie Deutschland GmbH & Co. KG. University of Bonn and AbbVie participated study design, research, interpretation of data, writing, data collection, analysis, reviewing, and approving the publication.

Declaration of Competing Interest

Barbara Schönfeld and Ulrich Westedt are employees of AbbVie and may own AbbVie stock. Barbara Schönfeld is a PhD student and Karl G. Wagner is a professor at the University of Bonn. They have no additional conflicts of interest to report.

Appendix A. Supplementary data

Supplementary data to this article can be found online at https://doi.org/10.1016/j.ijpx.2021.100102.

References

Agrawal, A.M., Dudhedia, M.S., Patel, A.D., Raikes, M.S., 2013. Characterization and performance assessment of solid dispersions prepared by hot melt extrusion and spray drying process. Int. J. Pharm. 457, 71–81. https://doi.org/10.1016/j.ijpharm.2013.08.081.

Bhandari, B., Bansal, N., Zhang, M., Schuck, P., 2013. 4.1 Introduction, Handbook of Food Powders - Processes and Properties. Woodhead Publishing.

Brunauer, S., Emmett, P.H., Teller, E., 1938. Adsorption of gases in multimolecular layers. J. Am. Chem. Soc. 60, 309–319. https://doi.org/10.1021/ja01269a023.

Davis, M.T., Potter, C.B., Walker, G.M., 2018. Downstream processing of a ternary amorphous solid dispersion: the impacts of spray drying and hot melt extrusion on powder flow, compression and dissolution. Int. J. Pharm. 544, 242–253. https://doi.org/10.1016/j.ijpharm.2018.04.038.

Dedroog, S., Huygens, C., Van den Mooter, G., 2019. Chemically identical but physically different: a comparison of spray drying, hot melt extrusion and cryo-milling for the formulation of high drug loaded amorphous solid dispersions of naproxen. Eur. J. Pharm. Biopharm. 135, 1–12. https://doi.org/10.1016/j.ejpb.2018.12.002.

Démuth, B., Nagy, Z.K., Balogh, A., Vigh, T., Marosi, G., Verreck, G., Van Assche, I., Brewster, M.E., 2015. Downstream processing of polymer-based amorphous solid dispersions to generate tablet formulations. Int. J. Pharm. 486, 268–286. https://doi.org/10.1016/j.ijpharm.2015.03.053.

Diarra, Harona, et al., 2015. Investigating the effect of tablet thickness and punch curvature on density distribution using finite elements method. International Journal of Pharmaceutics 493 (1), 121–128. https://doi.org/10.1016/j.ijpharm.2015.07.030.

Dobry, D.E., Settell, D.M., Baumann, J.M., Ray, R.J., Graham, L.J., Beyerinck, R.A., 2009. A Model-based Methodology for Spray-Drying Process Development. J. Pharm. Innov. 4, 133–142. https://doi.org/10.1007/s12247-009-9064-4.

Eiliazadeh, Brunel, et al., 2003. Investigating Density Distributions for Tablets of Different Geometry During the Compaction of Pharmaceuticals. Particulate Science and Technology 21, 303–306. https://doi.org/10.1080/716100572.

EMA/CHMP/ICH/82260/2006, 2019. ICH guideline Q3C (R6) on impurities: guideline for residual solvents EMA/CHMP/ICH/82260/2006.

FDA_Guidance, 1997. Guidance for industry dissolution testing of immediate release solid oral dosage forms. In: Research, C.f.D.E.A (Ed.), FDA-1997-D-0187. U.S. Department of Health and Human Services Food and Drug Administration.

Fell, J.T., Newton, J.M., 1970. Determination of Tablet Strength by the Diametral-Compression Test. J. Pharm. Sci. 59, 688–691. https://doi.org/10.1002/jps.2600590523.

Garner, Sean, et al., 2014. Mechanisms of crack formation in die compacted powders during unloading and ejection: An experimental and modeling comparison between

standard straight and tapered dies. Powder Technology 264, 114–127. https://doi.org/10.1016/j.powtec.2014.04.086.
Gold, G., Duvall, R.N., Palermo, B.T., Slater, J.G., 1966. Powder flow studies II: effect of glidants on flow rate and angle of repose. J. Pharm. Sci. 55, 1291–1295. https://doi.org/10.1002/jps.2600551125.
Haser, A., Cao, T., Lubach, J., Listro, T., Acquarulo, L., Zhang, F., 2017. Melt extrusion vs. spray drying: the effect of processing methods on crystalline content of naproxen-povidone formulations. Eur. J. Pharm. Sci. 102, 115–125. https://doi.org/10.1016/j.ejps.2017.02.038.
Heckel, R.W., 1961. Density-pressure relationships in powder compaction. Trans. Metall. Soc. AIME 221, 671–675.
Huang, S., Williams, R.O., 2018. Effects of the Preparation Process on the Properties of Amorphous Solid Dispersions. AAPS PharmSciTech 19, 1971–1984. https://doi.org/10.1208/s12249-017-0861-7.
Indulkar S., Anura, et al., 2019. Insights into the Dissolution Mechanism of Ritonavir–Copovidone Amorphous Solid Dispersions: Importance of Congruent Release for Enhanced Performance. Molecular Pharmaceutics 16 (3), 1327–1339. https://doi.org/10.1021/acs.molpharmaceut.8b01261.
Iyer, R., Hegde, S., Zhang, Y.-E., Dinunzio, J., Singhal, D., Malick, A., Amidon, G., 2013. The Impact of Hot Melt Extrusion and Spray Drying on Mechanical Properties and Tableting Indices of Materials used in Pharmaceutical Development. J. Pharm. Sci. 102, 3604–3613. https://doi.org/10.1002/jps.23661.
Lin, X., Hu, Y., Liu, L., Su, L., Li, N., Yu, J., Tang, B., Yang, Z., 2018. Physical Stability of Amorphous Solid Dispersions: a Physicochemical Perspective with Thermodynamic, Kinetic and Environmental Aspects. Pharm. Res. 35, 125. https://doi.org/10.1007/s11095-018-2408-3.
Mazel, V, et al., 2015. Lamination of pharmaceutical tablets due to air entrapment: Direct visualization and influence of the compact thickness. International Journal of Pharmaceutics 478 (2), 702–704. https://doi.org/10.1016/j.ijpharm.2014.12.023.
Neilly, J.P., Yin, L., Leonard, S.-E., Kenis, P.J.A., Danzer, G.D., Pawate, A.S., 2020. Quantitative measures of Crystalline Fenofibrate in Amorphous Solid Dispersion Formulations by X-Ray Microscopy. J. Pharm. Sci. 109, 3078–3085. https://doi.org/10.1016/j.xphs.2020.07.006.
Olsson, Helena, Nyström, Christer, 2001. Assessing Tablet Bond Types from Structural Features that Affect Tablet Tensile Strength. Pharmaceutical Research 18 (2), 203–210. https://doi.org/10.1023/A:1011036603006.
Patterson, J.E., James, M.B., Forster, A.H., Lancaster, R.W., Butler, J.M., Rades, T., 2007. Preparation of glass solutions of three poorly water soluble drugs by spray drying, melt extrusion and ball milling. Int. J. Pharm. 336, 22–34. https://doi.org/10.1016/j.ijpharm.2006.11.030.
Pitt, K.G., Heasley, M.G., 2013. Determination of the tensile strength of elongated tablets. Powder Technol. 238, 169–175. https://doi.org/10.1016/j.powtec.2011.12.060.
Polli, J.E., Rekhi, G.S., Augsburger, L.L., Shah, V.P., 1997. Methods to compare dissolution profiles and a rationale for wide dissolution specifications for metoprolol tartrate tablets. J. Pharm. Sci. 86, 690–700. https://doi.org/10.1021/js960473x.
Raghavan, R., Jett, J.L., 2004. Method to produce a solid form of heparin. In: International Application Published Under The Patent Cooperation Treaty. Pfizer Health AB.
Sangekar, S.A., Lee, P.I., Nomeir, A.A., 2003. Molecular Dispersion Composition with Enhanced Bioavailability, United States Patent. Schering Corporation.
Schönfeld, B., Westedt, U., Wagner, K.G., 2021. Vacuum drum drying – a novel solvent-evaporation based technology to manufacture amorphous solid dispersions in comparison to spray drying and hot melt extrusion. Int. J. Pharm. 596, 120233. https://doi.org/10.1016/j.ijpharm.2021.120233.
Shah, S., Maddineni, S., Lu, J., Repka, M.A., 2013. Melt extrusion with poorly soluble drugs. Int. J. Pharm. 453, 233–252. https://doi.org/10.1016/j.ijpharm.2012.11.001.
Tran, D.T., Majerová, D., Veselý, M., Kulaviak, L., Ruzicka, M.C., Zámostný, P., 2019. On the mechanism of colloidal silica action to improve flow properties of pharmaceutical excipients. Int. J. Pharm. 556, 383–394. https://doi.org/10.1016/j.ijpharm.2018.11.066.
Varthalis, S., Pilpel, N., 1977. The action of colloidal silicon dioxide as a glidant for lactose, paracetamol, oxytetracycline and their mixtures. J. Pharm. Pharmacol. 29, 37–40. https://doi.org/10.1111/j.2042-7158.1977.tb11234.x.
Vasconcelos, T., Marques, S., das Neves, J., Sarmento, B., 2016. Amorphous solid dispersions: Rational selection of a manufacturing process. Adv. Drug Deliv. Rev. 100, 85–101. https://doi.org/10.1016/j.addr.2016.01.012.